A multi-layer model for double-skin Pd-based membranes

Document Version:
Publisher's PDF, also known as Version of Record (includes final page, issue and volume numbers)

Please check the document version of this publication:

• A submitted manuscript is the version of the article upon submission and before peer-review. There can be important differences between the submitted version and the official published version of record. People interested in the research are advised to contact the author for the final version of the publication, or visit the DOI to the publisher's website.
• The final author version and the galley proof are versions of the publication after peer review.
• The final published version features the final layout of the paper including the volume, issue and page numbers.

Link to publication

A multi-layer model for double-skin Pd-based membranes: Layer-by-layer parameter fitting

W.J.R. Ververs [a], A. Arratibel [b], L. Di Felice [a], F. Gallucci [a,c,*]

[a] *Inorganic Membranes and Membrane Reactors, Sustainable Process Engineering, Department of Chemical Engineering and Chemistry, Eindhoven University of Technology, P.O. Box 513, 5600, MB Eindhoven, the Netherlands*
[b] *TECNALIA, Basque Research and Technology Alliance (BRTA), Mikeletegi Pasealekua 2, 20009, Donostia-San Sebastian, Spain*
[c] *Eindhoven Institute for Renewable Energy Systems (EIRES), Eindhoven University of Technology, P.O. Box 513, 5600, MB Eindhoven, the Netherlands*

ARTICLE INFO

ABSTRACT

The Pd-based double-skin (DS) membrane has high potential to be implemented in various industrial processes. However, its multi-layer structure makes it difficult to model and understand the limiting transport mechanisms through each of these layers. In this work an extensive set of experiments on several membranes with different configurations was performed with the purpose of deriving a detailed model for the double-skin Pd-based membrane. This is important for the general understanding of the mass-transport taking place within each of the membrane layers, namely the support, the selective and the protective layer. Characterization, permeation tests and data-fitting led to the construction and validation of a multi-layer model for the DS-membrane. The experimental results also pointed out that the protective layer of HT or YSZ/Al$_2$O$_3$ has only a minor or negligible effect on the overall transport resistance of the membrane. The influence of the support was found to be small but not negligible compared to the dominating resistance of the dense selective PdAg layer. Experiments and simulations of the membrane permeation in multi-component mixtures also highlighted the large importance of concentration polarization and H$_2$ depletion, which were successfully described in the model using a film-layer model together with a Sherwood correlation.

1. Introduction

Palladium-based membranes for hydrogen separation are a highly promising technology for processes where a high permeability and perm-selectivity for hydrogen is essential. A high perm-selectivity allows for a large hydrogen recovery in a small volume, which makes the Pd-based membranes an excellent option for integration in a compact membrane reactor system [1–8]. Various processes, like hydrocarbon reforming, hydrocarbon dehydrogenation, ammonia decomposition etc., are currently being developed to combine catalyst and Pd-based membranes in novel membrane reactor systems [9–18]. The use of a membrane reactor system can make many currently highly environmental impacting processes more energy and resource efficient [19–23]. The first and main advantage is that the membrane reactor can benefit from the Le Châtelier's principle, by removing reaction products and therefore shifting the equilibrium conversion towards the desired product. This shift of equilibrium conversion allows for a more compact design, both in size and in number of process units. Besides a high permeability like mentioned before, Pd-based membranes also bring a high perm-selectivity allowing for the elimination of any further downstream separation steps of the hydrogen product stream. Downstream product purification (especially the separation steps) is often a very energy intensive aspect of the process, so the use of Pd-based membranes has the potential to greatly improve the energy efficiency of a process involving hydrogen [1,24–26].

In the last two decennia, large steps have been made to improve hydrogen permeability and perm-selectivity of Pd-based membranes [5, 9,27,28]. The membranes have advanced from thick, self-supported Pd layers into ultra-thin supported Pd-alloy membranes [28]. Besides hydrogen permeability and perm-selectivity, membrane durability and stability are also important performance factors of the membranes. To enhance stability of the membrane in a catalytic membrane reactor, Arratibel et al. developed a so called "double-skin" (DS) membrane [29, 30]. This DS-membrane is a variant of a supported Pd-membrane with

an extra porous layer (protective layer) added on top of the PdAg layer (selective layer). The protective layer prevents contact between the selective layer and the catalyst. Therefore, the protective layer prevents undesired alloying between the catalyst and the selective layer, this could be useful in case of application in both a fixed and fluidized bed reactor. Besides that, erosion of the selective layer is reduced in fluidization conditions [29,30]. An additional advantage is the improved robustness of the membrane making the handling of the membranes safer, which is an advantage, especially towards industrial application. However, the membrane will be more expensive due to the extra steps in the production, but a longer membrane lifetime would anyway make the process more economical. Due to its superior properties, the double-skin PdAg membrane is currently being commercialized for application in processes like reforming and ammonia decomposition [31].

Even though the protective layer brings advantages to the membrane, the addition of an extra layer also increases the complexity of transport phenomena. Specifically in cases where concentration polarization or membrane deactivation takes place, it is important to properly understand the mass transfer behavior of the membrane. A first approach of modeling the DS Pd-based was done by Arratibel et al. by fitting the permeation data into Richardson's equation in a conventional Pd-based membrane. Richardson's equation can be found in Equation (1), it describes the hydrogen flux through a Pd-based membrane [32].

$$N = Q\left(p_{H_2,ret}^n - p_{H_2,perm}^n\right) \tag{1}$$

where Q is the permeance and n is the pressure exponent. With this approach, a higher value for the pressure exponent compared to the commonly observed value of 0.5 was found. A value of 0.5 is typically found in the case that the bulk diffusion step of the multi-step (solution-diffusion) mechanism is rate-limiting. However, in case other steps are limiting, for example external resistances from additional layers or surface phenomena, n can increase up to a maximum value of 1 [33–35]. With this approach, mass transfer resistances of the support, selective layer and protective layer are lumped as they would arise from a single layer. This pseudo-one-layer model is expected to have lower accuracy since the three layers have different mass transfer mechanisms and concentration polarization is not accounted for.

Brencio et al. modelled a DS-PdAg membrane in order to describe membrane deactivation in propane dehydrogenation conditions [36]. In this approach, Richardson's equation was used to describe the transport through the selective layer and the support. The pressure drop across the protective layer was accounted for using a simplified form of the dusty-gas model. For external concentration polarization, a film layer model with a Sherwood correlation for the mass transfer coefficient was incorporated. This approach is a large improvement compared to the work of Arratibel et al. but transport parameters for both external mass transfer and protective layer are based on estimations and validations of these parameters are lacking [37–39]. Besides that, also support resistance was not considered.

In this work a new and more detailed model will be developed and validated for the DS Pd-based membrane. Since the DS-membrane is a multi-layer membrane, it is difficult to quantify the contribution of each layer. Therefore, different membrane configurations have been used for permeation tests to collect data on the mass transport behavior through different layers of the DS-membrane. The obtained dataset was used for data fitting of the transport parameters required to predict the permeation properties of each layer. Finally, all the fitted parameters have been combined into one multi-layer model for the DS-PdAg membrane. An improved model for the DS-PdAg membrane can improve the understanding of the mass transport in each layer and it allows for better prediction of its behavior.

In the following work, the used materials and methods, including the membranes, characterization techniques, permeation tests and software will be introduced. In the next section, the model and its equations for each layer of the membrane will be described. Then in the results and

discussion, the outcome of the experiments and characterization, together with the acquisition of all the characteristic parameters necessary to complete the model will be presented. Finally, the model will be validated and demonstrated, followed by the conclusion. The dataset obtained from all the permeation tests is made available to other investigators in the supplementary materials and at Zenodo [40].

2. Materials and methods

2.1. Membrane preparation and activation

Different membranes and membrane configurations were used in this work, each membrane is assigned a code, like shown in Table 1.

The membranes were all prepared using porous asymmetric α-Al$_2$O$_3$ supports provided by Rauschert Kloster Veilsdorf. The pore size at the outer surface of the supports is 100 nm and it gradually decreases to 3.5 μm at the inner surface. Two different support sizes were used, namely with OD/ID ratio of 14/7 mm and 10/4 mm, as indicated in Table 2. For each membrane different deposition method(s) were applied. A schematic overview of the layers is given in Fig. 1.

Dual layer porous membranes S-HT and S-YSZ/Al$_2$O$_3$ were prepared by deposition of an extra porous layer directly on top of the porous support. Both the porous layers made of HT and YSZ/Al$_2$O$_3$ were deposited on the supports by dip coating of either a hydrotalcite sol or a YSZ/γ-Al$_2$O$_3$ mixed sol, respectively, followed by drying and calcination at 550 °C. The HT sol was obtained by peptization of hydrotalcite powder (PURAL MG30 supplied by Sasol) in nitric acid 0.4 M. The mixture was treated at 90 °C for 25 h for the complete peptization. More details of the preparation procedure of the YSZ/Al$_2$O$_3$ sol can be found in the work of Arratibel et al. [37]).

The Pd-based membranes were prepared by the (simultaneous) deposition of a PdAg or Pd layer on the α-Al$_2$O$_3$ support by electroless plating. The membranes were then washed with water, dried, and annealed at 550 °C for 4 h in 10/90% H$_2$/N$_2$. For the double-skin membranes (S–PdAg-HT and S–PdAg-YSZ/Al$_2$O$_3$), a third HT or YSZ/Al$_2$O$_3$ layer was deposited on top of the PdAg one, following a similar procedure as described above for the dual layer porous membranes [29]. The procedure was demonstrated successfully in various other works of Arratibel et al. [29,30,41].

Dimensions and general permeation characteristics of each H$_2$-selective Pd-based membrane can be found in Table 2.

All membranes containing a Pd-based layer were first activated in air for 2 min at 400 °C and then stabilized at 450 °C in pure H$_2$, after which permeation tests were performed.

Table 1
Overview of the different membranes used in this work.

Code	Description	Purpose
Porous membranes		
S	Porous Al$_2$O$_3$ support	Fitting support resistance
S-YSZ/Al$_2$O$_3$	Porous YSZ/Al$_2$O$_3$ on support	Fitting protective layer resistance
S-HT	Porous hydrotalcite on support	Fitting protective layer resistance
Conventional Pd-based membranes		
S–PdAg	Supported PdAg membrane	Validation external mass transfer
S–Pd	Supported Pd membrane	Validation external mass transfer
Double-skin Pd-based membranes		
S–PdAg-YSZ/Al$_2$O$_3$	DS-PdAg membrane with YSZ/Al$_2$O$_3$ protective layer	Validation overall model
S–PdAg-HT	DS-PdAg membrane with hydrotalcite protective layer	Validation overall model

Table 2

Table summarizing the important characteristics of each Pd-based membrane used in this work.

		S–PdAg-YSZ/Al$_2$O$_3$	S–PdAg-HT	S–PdAg	S–Pd
Length	mm	189	189	141	136
OD/ID	mm/mm	14/7	14/7	10/4	10/4
H$_2$ permeance[a]	mol s^{-1}m^{-2}bar^{-1}	0.211	0.122	0.362	0.345
H$_2$/N$_2$ Selectivity[a]	–	143,028	58,720	6,751	2,842

[a] 3 bar(a) and 400 °C.
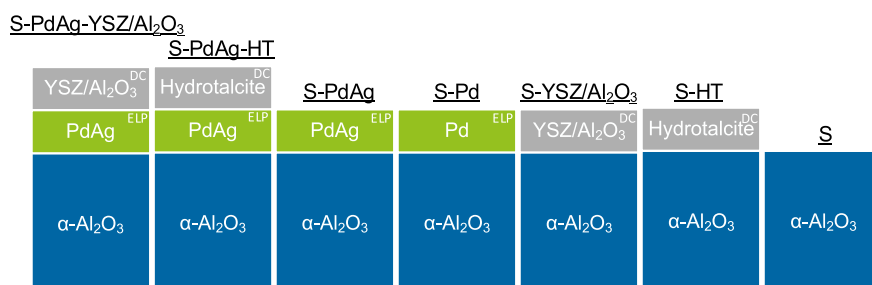
Fig. 1. Overview of the configuration of the different membranes used in this work. ELP = Electroless plating; DC = Dip coating. Membranes consist of combination of support (S, blue boxes), porous layers (HT and YSZ/Al$_2$O$_3$, grey boxes) and/or selective layers (PdAg and Pd, green boxes). Double-skin (DS) membranes (left) are characterized by a 3-layers structure.

2.2. Characterization

Before the membranes were used for permeation tests, a small fragment of the membrane was cut off and prepared such that the cross section could be scanned using Scanning Electron Microscopy (SEM). The images made using a FEI Quanta 250 FEG were used to measure the thickness of the different layers of each membrane.

N$_2$ physisorption was used for characterization of the porous structures of the nanoporous HT and YSZ/Al$_2$O$_3$ layers. The samples were prepared by drying the sols used for dip coating in a Petri dish and calcining the precipitate according to the same procedure of the porous membranes [37]. The N$_2$ physisorption was performed with a TriStar II 320 by Micromeritics.

2.3. Permeation tests

Permeation tests were performed using a membrane characterization setup where multiple membranes can be tested in identical experimental conditions. Schematic of the used permeation system is shown in Fig. 2. The Retentate pressure was controlled with a backpressure regulator provided by Bronkhorst, temperature was controlled using a Carbolite three-zone oven and feed flows were regulated by Bronkhorst mass flow controllers. The permeates of each membrane can be opened remotely to measure the permeation flow with either Bronkhorst mass flow meters or HORIBA film flow meters. The permeate pressure was always kept atmospheric.

Multiple membranes have been tested for their permeation properties under different conditions, e.g. the porous membranes have been tested in pure gas while the Pd-based membranes both in pure H$_2$ and H$_2$-containing mixtures. Full details of the adopted operating conditions during permeation tests are described in Table 3. The permeation flow was measured after temperature and flux were observed to be stable, for the tests with pure gases this was relatively fast, but for the tests with gas mixtures, this could take up to 10 min.

2.4. Model

The mathematical model was made using MATLAB R2021a software. Data fitting was done using the built-in *lsqnonlin* function, nonlinear equations were solved with *fsolve* and *ode45* was used as a numerical ode
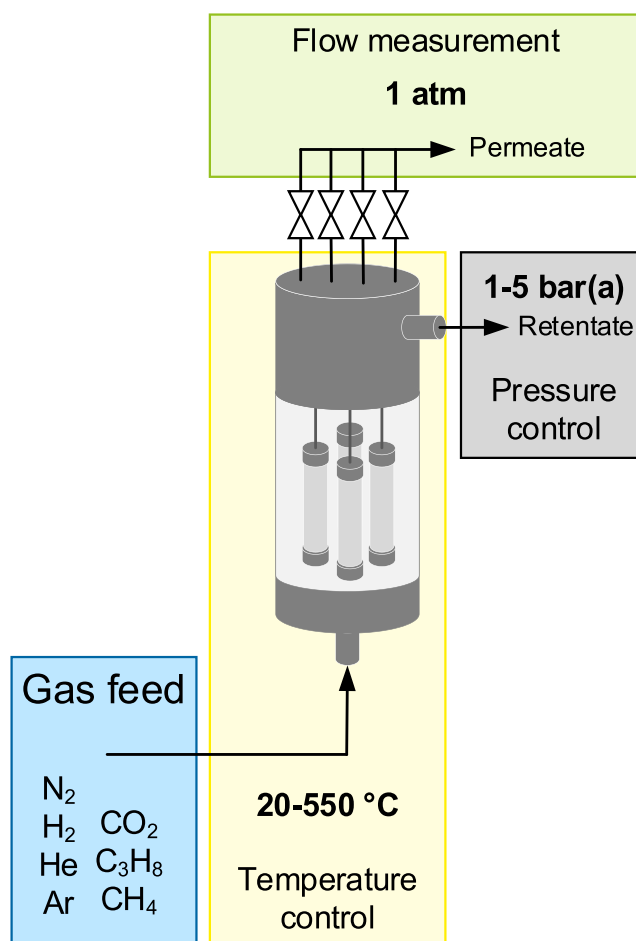

Fig. 2. Schematic representation of the used experimental setup.

Table 3
Details of the operative conditions adopted during permeation tests with the different membranes.

Membrane	Gas	T °C	p_{ret} bar(a)	$F_{v,feed}$ ln min^{-1}
S		20 − 500	1.5 − 5.0	*
	He; H_2; N_2; Ar; CH_4; CO_2; C_3H_8			
S-HT;		20 − 500	1.5 − 5.0	*
S-YSZ/Al$_2$O$_3$	He; H_2; N_2; Ar; CH_4; CO_2; C_3H_8			
S–PdAg; S–Pd;	H_2	350; 400; 450	1.5 − 5.0	*
S–PdAg-HT;S–PdAg-YSZ/Al$_2$O$_3$				
S–PdAg; S–Pd;		350; 400; 450	1.5 − 5.0	3; 5; 7
S–PdAg-HT;S–PdAg-YSZ/Al$_2$O$_3$	$H_2/N_2; H_2/Ar; H_2/Hex_{H_2,feed} = 0.7 − 0.9$			

* high enough to supply the permeating flow. In pure gas conditions, flowrate does not have any influence on the resulting permeation fluxes due to the absence of concentration polarization or depletion effects.

solver.

3. Model description

DS-membranes are distinguished by 3 different physical layers as can be seen in Fig. 3. First (from the external surface to the inside) a porous protective layer with a pore size expected in the nanoporous range is found [37]. A dense selective layer follows, where mass transport is typically described with a solution-diffusion mechanism. Finally, the support is depicted as a thick layer with decreasing pore size from the inside to the outside. Besides mass transfer resistance through the physical layers, gas phase external mass transfer resistance can also be a relevant contribution to the resulting permeation through the DS-membrane. Therefore, an external mass transfer layer is also considered in the model.

The transport of a multi-layer model is governed by its permeation parameters and the driving force in each layer, which in turn is determined by the hydrogen partial pressure at each side as shown in Fig. 3. The partial pressures at the interfaces of each layer are calculated using transport models for each of the layers – selected based on the governing transport mechanisms as discussed below.

In the model, a few basic assumptions were made. The bulk gas phase around the membrane was modelled as 1D plug flow, being discretized in the axial direction. The membrane was also modelled in the radial direction since the pressure profile through the layers of the membrane was calculated for each axial position. The system has been treated as completely isothermal, since during the experiments, the temperature difference along the length of the membranes was kept smaller than

5 °C. The membrane module was tested and modelled without the presence of any particles and without a sweep gas on the permeate side.

3.1. Support layer

As previously described, the porous support has a pore size distribution that varies in the radial direction, so various transport mechanisms are expected to take place at the same time. To determine which transport mechanisms are taking place inside the support, the calculation of the Knudsen number can indicate which mechanisms are relevant in the specified conditions. In Figure 18 of Appendix 5, a plot of the calculated Knudsen number and pore size is given, indicating the pore size range specified for the support. The calculated Knudsen numbers indicate that viscous, slip and transition flow can be taking place inside the support. Therefore, a permeation model able to predict the behavior in these overlapping transport regimes is required.

The dusty-gas model is the most commonly applied model for transport in porous media when multiple transport mechanism are taking place, since it considers both a viscous (continuum) and a Knudsen (free molecular) term [42–44]. The intermediate regimes (slip and transition flow) can be accounted for by tuning the viscous and Knudsen contributions. In Equation (2), the dusty-gas model for a 1-component system can be found. The 1-component form of the dusty-gas model is sufficient in the case that no sweep gas is used, since only H_2 is present in the permeate side of the membrane, assuming that the selectivity is sufficiently large that the permeation of species other than H_2 can be neglected.
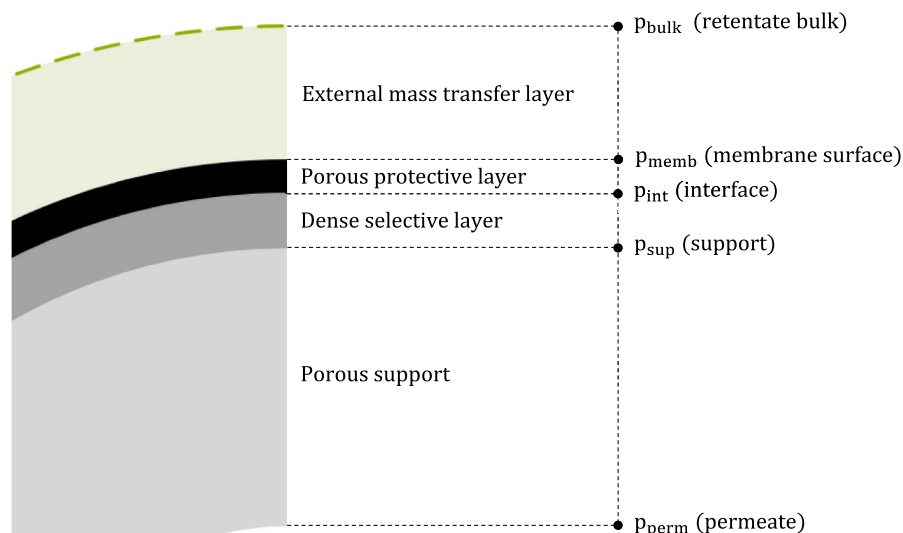

Fig. 3. Different layers included in the DS Pd-based membrane model.

$$N_i = - \frac{1}{RT} \left(\frac{4}{3} K_0 \sqrt{\frac{8RT}{\pi M_i}} + \frac{B_0 p}{\mu_i} \right) \frac{\partial p_i}{\partial y} \tag{2}$$

K_0 and B_0 are the characteristic parameters, which depend on the geometry of the porous structure [45].

3.2. Protective layer

The protective layer is, just like the support, a porous layer contributing to the transport resistance of the DS-membrane. However, compared to the support, the protective layer is in contact with a mixture of gases, meaning that a multi-component model must be used for this layer. The multi-component dusty-gas model equations are used to model this layer as shown below.

$$\sum_{\substack{j=1 \\ j \neq i}}^{n} \frac{x_i N_j - x_j N_i}{p D_{ij}^e} - \frac{N_i}{p D_{Kn,i}^e} = \frac{1}{RT} \frac{\partial x_i}{\partial y} + \frac{x_i}{p RT} \left(\frac{B_0 p}{\mu D_{Kn,i}^e} + 1 \right) \frac{\partial p}{\partial y} \tag{3}$$

$$D_{i,k}^e = \frac{4}{3} K_0 \sqrt{\frac{8RT}{\pi M_i}} \tag{4}$$

$$D^e = \frac{\varepsilon}{\tau} D \tag{5}$$

To use the multi-component dusty-gas model, the characteristic parameters of the dusty-gas model (K_0 and B_0) must be known. Besides that, also the thickness of the layer and the ratio of porosity and tortuosity are important. The ratio of porosity and tortuosity can be estimated using the expression for K_0 in capillary pores and the fitted K_0 value as well as the pore diameter obtained from the N_2 physisorption analysis [46].

$$K_0 = \frac{\varepsilon}{\tau} \frac{d_p}{4} \rightarrow \frac{\varepsilon}{\tau} = \frac{4 K_0}{d_p} \tag{6}$$

3.3. Selective layer

The selective layer of the DS-membrane consists of a thin PdAg layer. The transport mechanism through this layer is solution-diffusion, which for Pd-based membranes is commonly described using Richardson's equation:

$$N_{H_2} = Q_0 \exp \left(-\frac{E_a}{RT} \right) \left(p_{H_2,int}^n - p_{H_2,sup}^n \right) \tag{7}$$

where Q_0 is the pre-exponential factor, E_a the activation energy and n the pressure exponent. Permeability, activation energy, pre-exponential factor and pressure exponent are strongly correlated to the surface properties and thickness of the layer [35].

3.4. External mass transfer layer

Concentration polarization and H_2 depletion have large impacts on the overall membrane performance and are therefore essential to be included in a multi-component membrane model [47]. In this work, a multi-component gas-phase mass transfer model has been added where the membrane and gas-phase is discretized in the axial direction to account for H_2 depletion due to permeation. The mass balances over each cell can be found in Appendix 1, one for H_2 and one for all other components.

To calculate the external mass transfer rate, a film layer model was used, as described by Ververs et al. [47]. The used equations are also reported in Appendix 1. To describe the mass transfer coefficient, the use of a suitable Sherwood correlation is required. Viscosity and difusivity

have been calculated following the description in Appendix 2 [48–50].

4. Results and discussion

In this section, the parameters defining the transport rates in the membranes layers will be derived using characterization and modeling methods and tools previously described, as well as comprehensive datasets obtained from permeation tests.

4.1. Characterization

N_2 physisorption was performed to measure the pore size distribution of the protective layer. Samples were prepared according to the procedure in the experimental section. In Fig. 4A, the calculated pore size distribution based on the N_2 physisorption tests is shown. For the YSZ/Al_2O_3, the pore size varies in the range of 1–5 nm. This corresponds to observations of Arratibel et al. on the analysis of similar layers [37]. For the hydrotalcite material, pores of 2–70 nm are observed. These pore sizes can be used to calculate the Knudsen number, shown in Fig. 4B, which gives an indication of the flow regime. Based on the calculated Knudsen numbers, free-molecular flow behavior is expected for the YSZ/Al_2O_3 material. For the hydrotalcite layer, besides free-molecular flow, also transitional flow behavior can be expected.

The thicknesses of each of the membrane layers were determined by using SEM on the cross section, as shown in Fig. 6. S-HT and S-YSZ/Al_2O_3 have layers of 1.85 and 1.86 μm respectively. The DS-membranes S–PdAg-HT and S–PdAg-YSZ/Al_2O_3 have selective layers of 5.36 and 6.27 μm, and protective layers of 1.20 and 1.00 μm. The conventional Pd-based membranes S–Pd and S–PdAg have selective layer thicknesses of 2.14 and 2.83 μm.

4.2. Parameter fitting

4.2.1. Support

Permeation tests in pure H_2 at different temperatures and pressures were first performed with a support alone (S). The dusty-gas model (Equation (2)) was selected to describe the transport in the porous support. The characteristic parameters were fitted using the obtained dataset for three different cases: 1) including both the viscous and the Knudsen terms; 2) including only the viscous term; 3) including only the Knudsen term.

The resulting parameters shown in Table 4 are compared to the experimental data in Fig. 6. The comparison shows that including both the viscous and Knudsen terms leads to the best fit with the experimental data. This is in line with the calculations of the Knudsen number, showing that several different flow regimes are present inside the porous structure of the support.

4.2.2. Protective layer

A set of permeation experiments using porous membranes S-HT and S-YSZ/Al_2O_3 was performed to obtain dataset that can be used to fit the transport parameters of the protective layer. These transport parameters are required to describe the mass transport in the porous layers using the dusty-gas model (Equation (2)). Since the layer deposition procedure of these membranes is the same as the procedure for deposition of the protective layer on a DS-PdAg membrane, it can be assumed that the layer deposited on the support is representative for the protective layer of a DS-PdAg membrane [29,37].

Fig. 7 shows permeation data of the blank support, supported hydrotalcite and supported YSZ/Al_2O_3 membranes for H_2 and N_2 at 400 °C. The graph shows that the support and the supported hydrotalcite layer have identical resistance, meaning that the hydrotalcite layer has a negligible mass transport resistance compared to the support. This means that the HT layer can be neglected in the overall DS-membrane model. However, the S-YSZ/Al_2O_3 layer shows a lower flux compared to the blank support, indicating that the addition of a YSZ/Al_2O_3
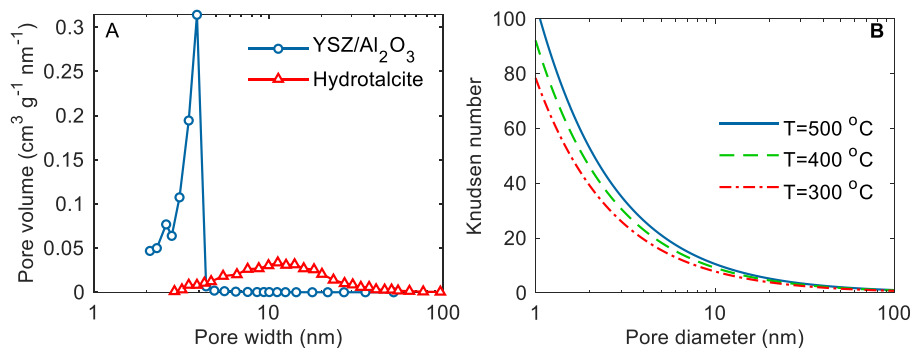
Fig. 4. A) Pore size distributions calculated from N_2 physisorption data. B) Plot of Knudsen number for varying pore diameter, calculated for H_2 at 3 bar(a).
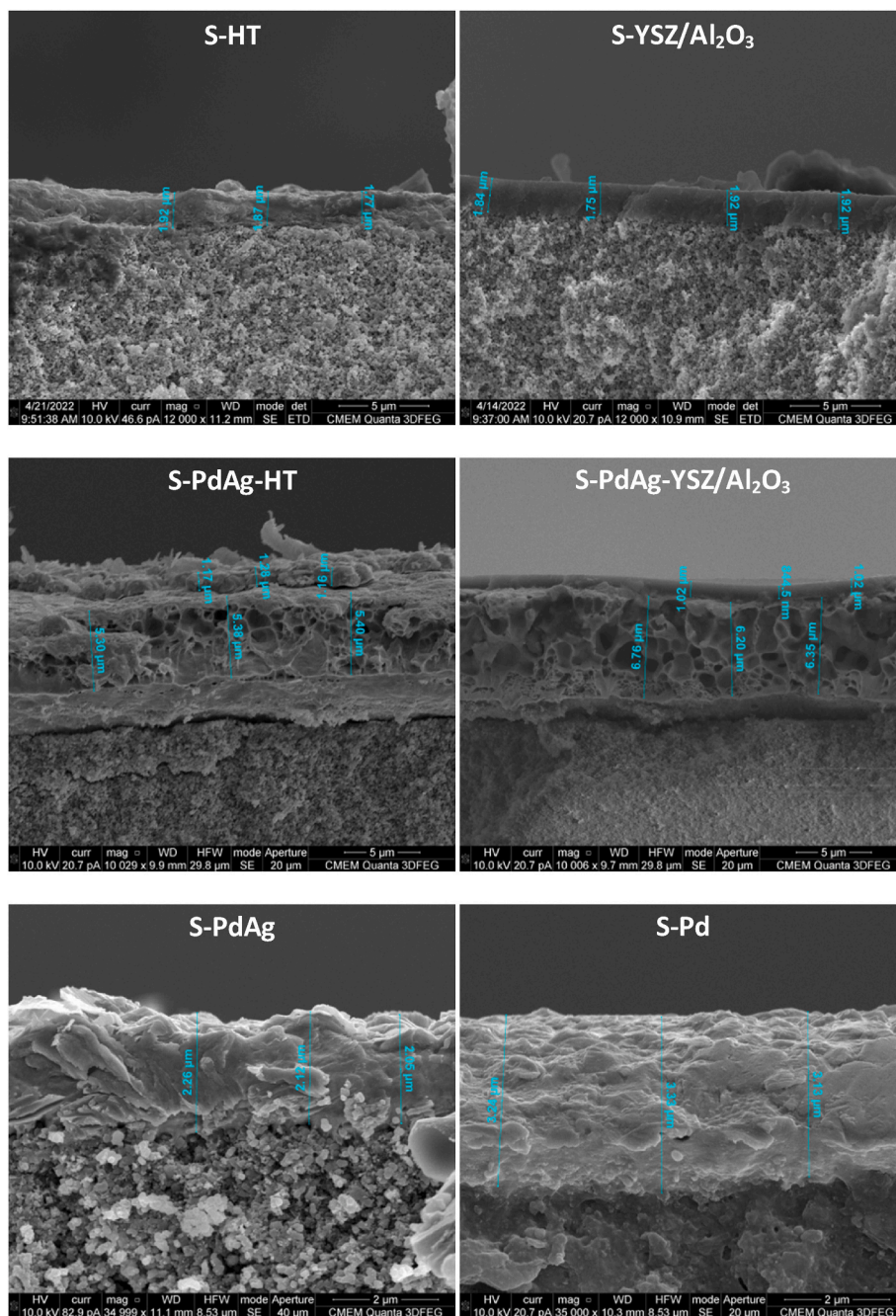

Fig. 5. Images made by SEM of the cross-section of S-HT, S-YSZ/Al_2O_3, S–PdAg-HT, S–PdAg-YSZ/Al_2O_3, S–PdAg and S–Pd.
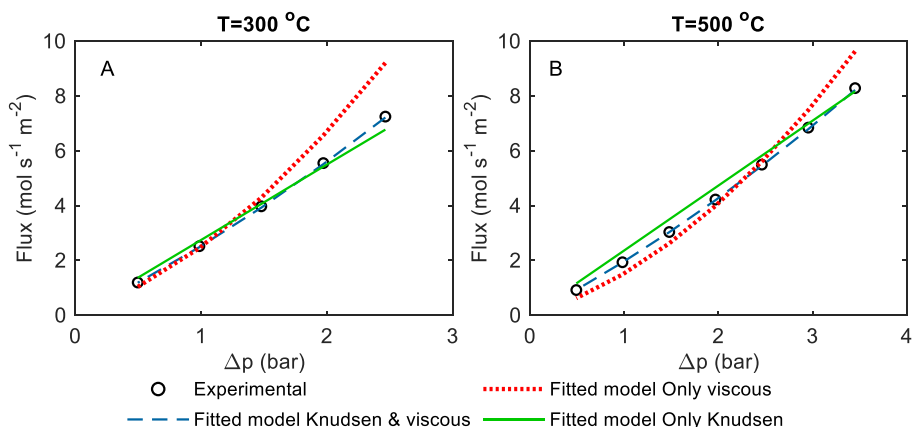
Fig. 6. Fitting results of support characteristic parameters in different cases compared to experimental results of H_2 permeation at 300 and 500 °C.

Table 4
Fitted values of the dusty-gas model equations for the different cases for the porous support.

	B_0 (m^2)	K_0 (m)	R^2 $(\%)$
Only Knudsen term	0	1.402×10^{-7}	94.80
Only viscous term	4.036×10^{-14}	0	55.13
Both Knudsen and viscous terms	1.315×10^{-14}	8.723×10^{-8}	99.95

Table 5
Fitted values of the dusty-gas model equations for the different cases for the YSZ-Al_2O_3 layer.

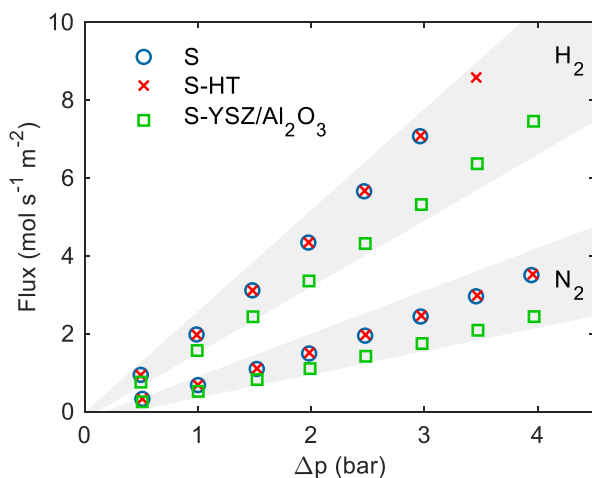|	B_0 (m^2)	K_0 (m)	R^2 $(\%)$
Only Knudsen term	0	2.671×10^{-10}	99.94%
Only viscous term	1.904×10^{-17}	0	87.38%
Both Knudsen and viscous terms	6.560×10^{-19}	2.606×10^{-10}	99.95%

Fig. 7. Permeation flux against *trans*-membrane pressure difference for tests performed at 400 °C with H_2 and N_2.

increases the transport resistance significantly.

To derive the transport parameters of the YSZ/Al_2O_3 layer, the permeation data must be compensated with the pressure drop over the support. To achieve this, the dusty-gas model parameters for each component were fitted using the permeation data of the support (S) alone in identical conditions as the S-YSZ/Al_2O_3 membrane. The used support parameters can be found in Appendix 5.

The same approach adopted for the support can be extended here identify which transport phenomena are important, the data fitting was done in three different cases, including only the Knudsen term ($B_0 = 0$ & $K_0 > 0$), only the viscous term ($B_0 > 0$ & $K_0 = 0$) or both terms (B_0 & $K_0 > 0$) of the dusty-gas model. The resulting values from the fitting can be found in Table 5.

In Fig. 8, a sample of the experimental results from the S-YSZ/Al_2O_3 membrane using the corrected pressure drop over the YSZ/Al_2O_3 layer is

shown. The experimental data is compared to three different fitting cases including only the Knudsen term ($B_0 = 0$ & $K_0 > 0$), only the viscous term ($B_0 > 0$ & $K_0 = 0$) or both terms (B_0 & $K_0 > 0$) of the dusty-gas model. The results show that there is practically no difference between the case with both terms included and the case with only the Knudsen term included. This means that including the viscous term is unnecessary, since contributions of viscous, slip and transition flow are negligible. This is in line with the Knudsen numbers calculated by using the pore size distribution obtained by N_2 physisorption, indicating that free-molecular transport is expected in the nanopores.

Additional permeation tests were performed for S-YSZ/Al_2O_3 with C_3H_8, CH_4 and CO_2 (20–400 °C). It should be noted that tests with C_3H_8 were only performed up to 200 °C, to prevent the deposition of any carbonaceous species on the ceramic membrane. The data obtained with these gases was not used for the fitting dataset, rather to validate the model and the fitted parameters outside the fitted conditions. Fig. 9 shows the box plots of the relative error of the model with the fitted parameters for both the support and the YSZ/Al_2O_3 layer. The relative error (RE) was calculated according to the following equation.

$$RE = \frac{N_{pred} - N_{exp}}{N_{exp}} \times 100\% \tag{8}$$

Fig. 9A shows that the error in the prediction of the support resistance is negligible and therefore it should not present any additional error in the prediction of the support's resistance. Fig. 9B shows the box plots of the relative error of the model with the fitted parameters for the nanoporous layer and support. The graph shows that the model is quite accurate for the dataset of 300–400 °C, which represents the relevant temperature range of the DS-PdAg membrane, as stable operation of Pd-based membranes is typically limited to a temperature range of 300–525 °C [5]. At lower temperature, the fitted parameters do not show a good agreement with experimental data. To show that this error does not come from the support resistance, the box plot of the relative error by the support model in identical conditions can be found in Fig. 9A. The error of the support model is very small, since the parameters re fitted for each component separately. Therefore, it is certain that the error observed at low temperature for the S-YSZ/Al_2O_3 model is
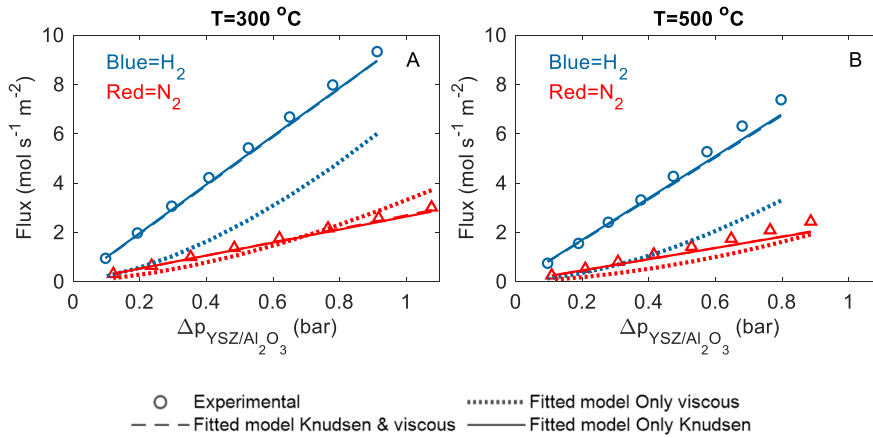
Fig. 8. Comparison of fitting results of the YSZ/Al$_2$O$_3$ layer transport model with experimental data compensated for support pressure drop, A) at 300 °C and B) at 500 °C.
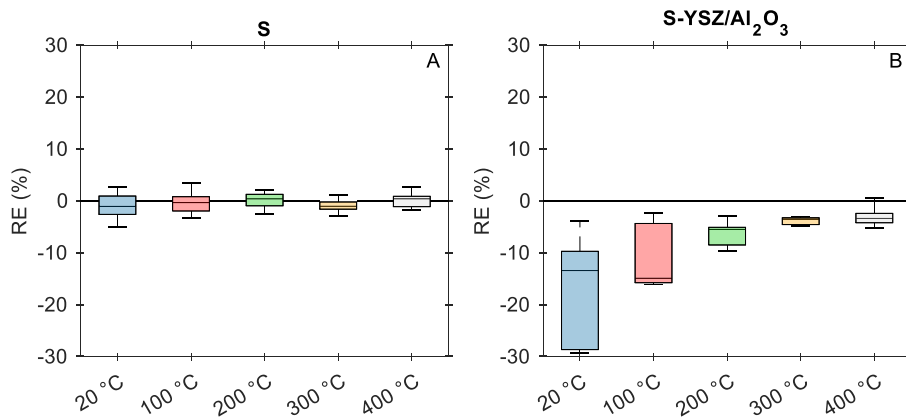

Fig. 9. Box plot showing the relative error of: A) the fitted and experimental data of the support (S) model and B) the experimental validation data and the model's predictions for the YSZ/Al$_2$O$_3$ layer model. The experimental data was obtained in pure C$_3$H$_8$, CH$_4$ and CO$_2$, at T = 20–400 °C and 1.5–4 bar(a).

coming from the nanoporous layer and not from the support. A possible reason for this error can be the way that the dusty-gas model deals with the intermediate flow regimes (i.e. slip flow and transition flow), namely subdividing them between the viscous and Knudsen term. This could possibly lead to an error when applying the model for gases with different properties than the gases used for parameter fitting.

4.2.3. Selective layer

To obtain the permeation parameters of Richardson's equation (Equation (7)), a set of experimental datapoints in pure H$_2$ at different pressures and temperatures was performed with each Pd-based membrane used in this work. The transport parameters (Q$_0$, E$_a$ and n) of the selective layer were fitted while accounting for the resistance of the support and the protective layer according to the transport parameters fitted in the previous sections.
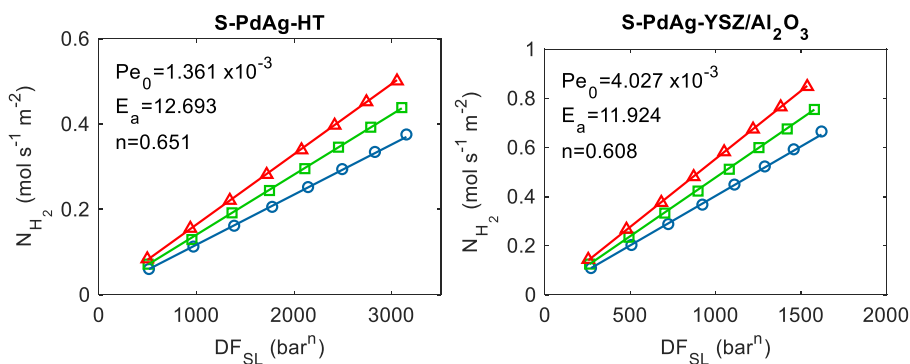

Fig. 10. Pure H$_2$ permeation plots, including the fitted Richardson parameters for S–PdAg-YSZ/Al$_2$O$_3$ and S–PdAg-HT. Tests were performed in pure H$_2$ with varied pressure and temperature.

In Fig. 10, the results of data fitting of the Richardson parameters of the selective layers of the DS-membranes are shown. For the sake of completeness, the graphs for S–PdAg and S–Pd can be found in Appendix 3, while the parameters and thickness for each layer (Fig. 5) of each Pd-based membrane are reported in Table 6. The Richardson parameters of the selective layer complete the set of transport parameters for the three physical layers of the DS-membrane. In Appendix 3, a parity plot for the permeation flux predicted by the model and observed in the experiments can be found for each DS-membrane. This indicates that the model is properly predicting the permeation behavior in pure H_2 conditions.

4.2.4. External mass transfer

To describe external mass transfer around the membrane, the film-layer model (Appendix 1) was used, but the calculation of the mass transfer coefficient requires the use of a suitable Sherwood correlation. Three different correlations from literature used for a single Pd-based membranes in an empty vessel were implemented in the model [35, 36,38,39,47]. To evaluate the accuracy each of these empirical correlations was implemented in the model and compared to results of the mixture tests performed with two conventional membranes (S–Pd and S–PdAg) in identical conditions as the tests performed with the DS-membranes. Fig. 11A shows a boxplot comparing the accuracy of each correlation in terms of relative error compared to the experimental dataset. The boxplot clearly indicates that the first correlation by Ververs et al. (given in Equation (9)) is the most accurate for the system/configuration used in this work [47].

$$Sh_z = 1.846 \bullet Gz_z^{0.60} \tag{9}$$

$$k_{g,i} = \frac{Sh \bullet d_h}{D_{i,mix}} \tag{10}$$

In Fig. 11b, the parity plot for the results obtained for the conventional membranes and the prediction by the model using the Sherwood correlation (Equation (9)) is given. The results show that the model gives some error, but it is smaller than 10% for most of the datapoints, which compares well with typical errors obtained by using Sherwood correlations from literature [47].

Table 6
Overview of all fitted membrane parameters for each Pd-based membrane used in this work.

Membrane	Support	Selective layer	Protective layer
S–PdAg-YSZ/Al₂O₃	$t = 3.5$ mm	$t = 6.27\ \mu m$	$t = 1.00\ \mu m$
			$K_0 = 2.671 \times 10^{-10}$
	$K_0 = 8.723 \times 10^{-8}$ $B_0 = 1.315 \times 10^{-14}$	$Q_0 = 4.027$ $E_a = 11.924 n = 0.608$	$B_0 = 0$
S–PdAg-HT	$t = 3.5$ mm	$t = 5.36\ \mu m$	$t = 1.20\ \mu m$ Neglected
	$K_0 = 8.723 \times 10^{-8}$ $B_0 = 1.315 \times 10^{-14}$	$Q_0 = 1.361$ $E_a = 12.693 n = 0.651$	
S–PdAg	Not accounted[a]	$t = 2.83\ \mu m$	
		$Q_0 = 2.473$ $E_a = 8.587 n = 0.628$	
S–Pd	Not accounted[a]	$t = 2.14\ \mu m$	
		$Q_0 = 3.583$ $E_a = 9.392 n = 0.607$	

$[K_0] =$ m; $[B_0] =$ m²
$[Q_0] = \times 10^{-3}$ mol s⁻¹m⁻²Pa⁻ⁿ; $[E_a] =$ kJ/mol
[a] Support was not accounted since S–PdAg and S–Pd have 10/4 supports and this support was not characterized in this work.

4.2.5. Overall model validation

Since all the layers of the membrane and external mass transfer have been modelled, the completed model for the DS-membrane can be used for simulations and compared to permeation results obtained from the mixture tests with S–PdAg-HT and S–PdAg-YSZ/Al₂O₃. The parameters from Table 6 were used together with the Sherwood correlation for external mass transfer in Equation (9). Fig. 12 shows the parity plot for the predicted and experimentally observed fluxes for the DS-membranes. The model is relatively accurate at predicting the flux of the DS-membrane, errors are laying mostly within the 10% error margin. It is expected that most of the observed error is caused by the prediction of the external mass transfer rates. These external mass transfer rates towards highly permeable membrane surfaces are typically very difficult to predict, for various reasons. High (radial) convective mass transfer rates towards the membrane surface lead to a distorted velocity profile, in addition to entrance effects occurring due to developing flow when the gas flow is contacted with the membrane surface [47].

4.2.6. Simulations

In addition, the model calculates the pressure drop through each layer of the membrane, allowing to evaluate the distribution of the mass transfer resistances. In Fig. 13, a bar chart with the pressure drop of each layer with varying N_2 dilution is visualized. The largest contributions to the pressure drop are the selective layer and the external mass transfer layer. The contribution of the support is small but not negligible, however the contribution of the protective layer is barely visible in the bar chart and can therefore be considered as negligible.

Fig. 14 shows the results of a simulation varying the *trans*-membrane pressure difference. The model was used to observe the effect of different phenomena determining the permeation flux: dilution, H_2 depletion and concentration polarization (CP). An increasing pressure difference makes depletion and concentration polarization significantly more important. A higher pressure difference leads to a higher hydrogen recovery factor, which is practically coincident with H_2 depletion. A higher flux causes the external mass transfer step to become mostly rate determining, since the radial dispersion in the gas phase around the membrane is limited.

Fig. 15 shows the effect of the feed flow rate (at constant inlet composition) on the permeation flux predicted with the DS-membrane model. Dilution is obviously not affected, but depletion and concentration polarization are strongly dependent by the feed flow rate. Depletion reduces with the feed flow rate since, at a higher feed flow rate the HRF decreases since there is less membrane area relative to the supply of hydrogen. Also concentration polarization decreases for a higher feed flowrate since a higher gas velocity improves radial dispersion.

5. Conclusions

A new model was developed to describe the flux through double-skin PdAg membranes. The model was derived by applying a layer-by-layer parameter fitting approach, including the gathering of an experimental dataset, parameter fitting and model validation. First, extensive experimental tests were performed on a range of different multi-layer membrane configurations. Permeation tests were done using a support, a supported hydrotalcite (HT) and YSZ/Al₂O₃ porous layer membrane. The permeation behavior and predicted pore size range indicated that various permeation flow regimes take place inside the support. Therefore, the dusty-gas model has been selected to describe the mass transfer in the support. The transport parameters were fitted to accurately describe the H_2 transport. The analysis and permeation tests of the nanoporous HT and YSZ/Al₂O₃ layers showed that mass transfer resistance of the HT layer is negligible compared to the resistance of the support. For the YSZ/Al₂O₃ layer, the observed mass transfer behavior was governed by Knudsen transport, which is in line with the predictions based on the pore size distribution. The Richardson parameters of the
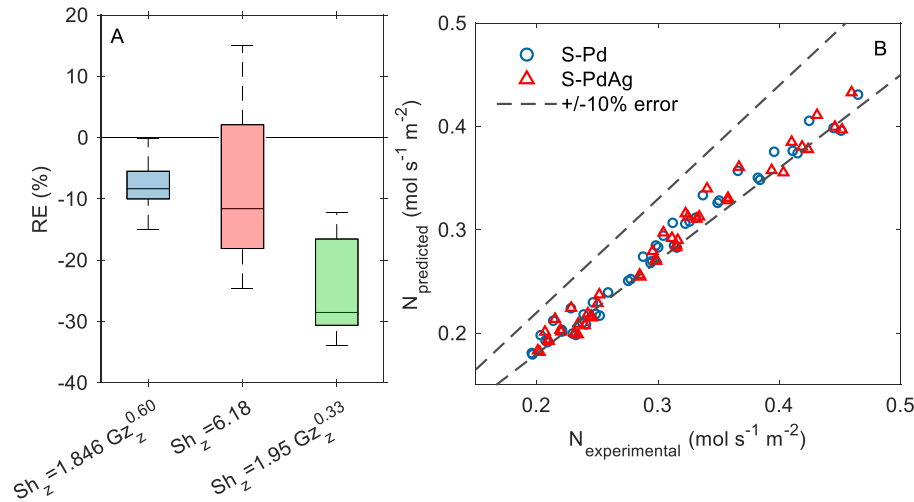
Fig. 11. A) Boxplot showing the comparison of three different Sherwood correlations adopted from literature. B) Parity plot showing experimental fluxes obtained for S–Pd and S–PdAg mixture tests and predicted fluxes using the most suitable Sherwood correlation by the model.
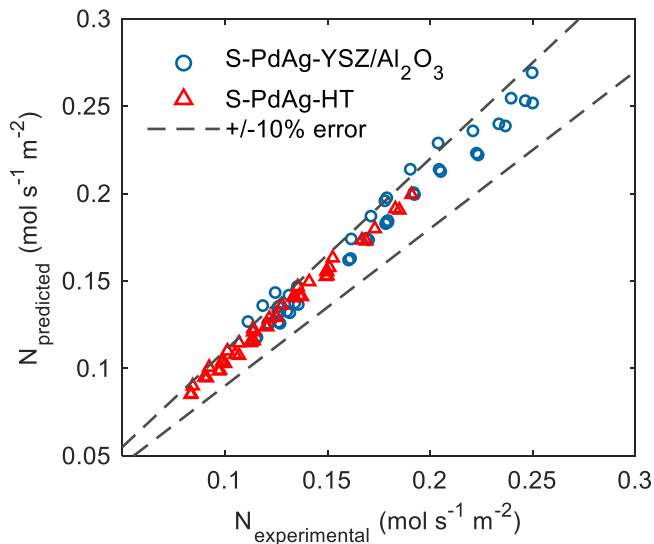

Fig. 12. Parity plot showing experimental fluxes obtained for S–PdAg-YSZ/Al$_2$O$_3$ and S–PdAg-HT mixture tests and predicted fluxes by the model.
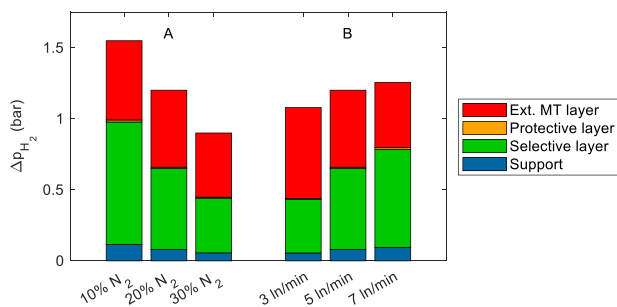

Fig. 13. Bar chart showing the pressure drop for each layer of the DS-PdAg-YSZ/Al$_2$O$_3$. A) 5 ln/min, 400 °C and 3 bar(a). B) 20% N$_2$, 400 °C and 3 bar(a).
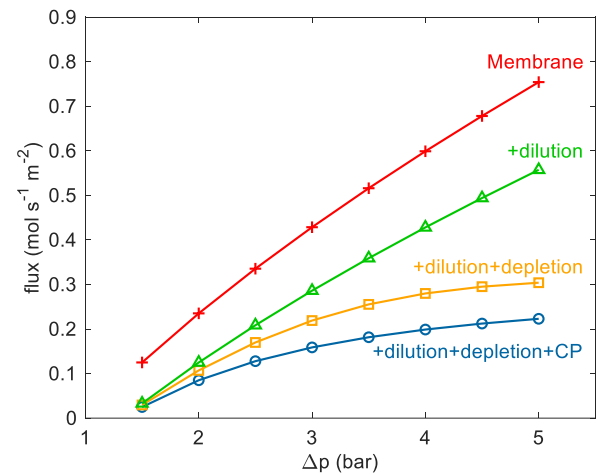

Fig. 14. Permeation flux versus *trans*-membrane pressure difference predicted by the model with different flux-limiting effects included. Simulation was performed at 400 °C, 0.75/0.25H$_2$/N$_2$ and 5 ln min^{-1}.

selective Pd-based layer were fitted, while accounting for the resistance of the porous support and protective layer. Finally, external mass transfer was described using a film layer model with a Sherwood correlation to calculate the mass transfer coefficient. A set of permeation tests in different mixtures was performed with two conventional membranes to evaluate the accuracy and applicability of some different Sherwood correlations available in literature. The correlation by Ververs et al. was selected due to its superior accuracy in combination with the membrane module used in this work. Finally, the newly developed model was validated using a set of experimental tests performed with two different double-skin membranes. The validation showed that the accuracy of the model is mostly within 10% error in the tested conditions. Since the model calculates the pressure at the interface between each of the layers, the pressure profile could be analyzed, giving a good view of the distribution of the mass transfer resistance. Most mass transfer resistance in the membrane is induced by the selective and external mass transfer layers. The support has only a minor contribution and the protective layer is negligible.

This work constructed, fitted, and validated a new and detailed model to describe the mass transport of double-skin PdAg membranes.
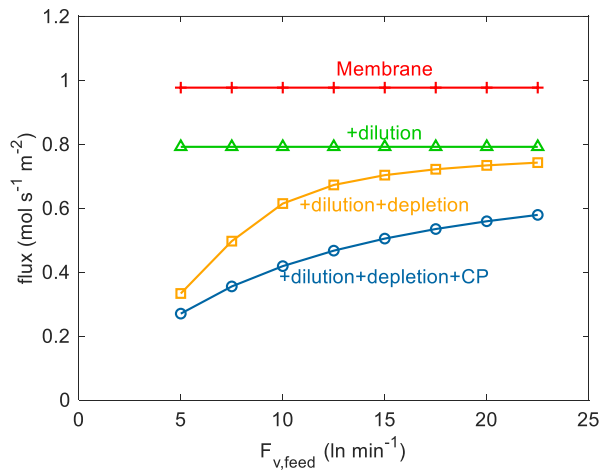
Fig. 15. Permeation flux versus feed flow rate predicted by the model with different flux-limiting effects included. Simulation was performed at 400 °C, $0.75/0.25 H_2/N_2$ and Δp of 4.9 bar.

An extensive experimental dataset was used to determine the critical parameters of the model. The permeation data of the tests of each membrane is made available for other investigators at Zenodo.

CRediT authorship contribution statement

W.J.R. Ververs: Conceptualization, Formal analysis, Methodology, Software, Writing – original draft, Writing – review & editing. **A. Arratibel:** Methodology, Resources, Writing – original draft. **L. Di Felice:** Supervision, Writing – review & editing. **F. Gallucci:** Conceptualization, Funding acquisition, Project administration, Supervision, Writing – review & editing.

Declaration of competing interest

The authors declare that they have no known competing financial interests or personal relationships that could have appeared to influence the work reported in this paper.

Acknowledgments

Appendix A. Supplementary data

Supplementary data to this article can be found online at https://doi.org/10.1016/j.ijhydene.2024.05.225.

Nomenclature

Letters

A	Membrane area m^2
B_0	Viscous flow parameter m^2
d_{col}	Collision diameter m
d_p	Pore size m
d_h	Hydraulic diameter m
D	Diffusion coefficient $m^2\ s^{-1}$
D_{Kn}	Knudsen diffusivity $m^2 s^{-1}$
DF	Driving force bar^n
E_a	Activation energy $J\ mol^{-1}$
F_v	Volumetric flow $ln\ min^{-1}$
F	Molar flow $mol\ s^{-1}$
Gz	Graetz number
HRF	Hydrogen recovery factor %
i	Specified component
ID	Inner diameter mm
k_B	Boltzmann constant $J\ K^{-1}$
k_g	Mass transfer coefficient $m\ s^{-1}$
K_0	Knudsen flow parameter m
Kn	Knudsen number
M	Molar mass $kg\ mol^{-1}$
n	Pressure exponent
N	Molar flux $mol\ s^{-1}\ m^{-2}$
OD	Outer diameter mm
p	(Partial) pressure Pa
Q	Permeance $mol\ s^{-1} m^{-2} Pa^{-n}$
Q_0	Pre-exponential factor of permeance $mol\ s^{-1} m^{-2} Pa^{-n}$
r	Radius m
R	Universal gas coefficient $J\ mol^{-1} K^{-1}$
Re	Reynolds number
RE	Relative Error %
Sc	Schmidt number

Sh   Sherwood number
t   Thickness m
T   Temperature K
x   Molar fraction
y   Radial coordinate m
z   Axial coordinate m

Greek letters

δ   Layer thickness m
ε   Porosity
λ   Mean free path m
μ   Dynamic viscosity Pa s
ρ   Mass density kg m^{-3}
τ   Tortuosity

Subscripts

exp   experimental
int   Interface
memb   membrane
mix   Relative to mixture
perm   Permeate
pred   Predicted
ret   Retentate
sup   support
SL   Selective layer

References

[1] Paglieri SN, Way JD. Innovations in palladium membrane research. Separ Purif Methods 2002;31(1):1–169. https://doi.org/10.1081/SPM-120006115.
[2] Kikuchi E. Membrane reactor application to hydrogen production. Catal Today 2000;56(1–3):97–101. https://doi.org/10.1016/S0920-5861(99)00256-4.
[3] Quicker P, Höllein V, Dittmeyer R. Catalytic dehydrogenation of hydrocarbons in palladium composite membrane reactors. Catal Today 2000;56(1–3):21–34. https://doi.org/10.1016/S0920-5861(99)00259-X.
[4] Dittmeyer R, et al. Micro and micro membrane reactors for advanced applications in chemical energy conversion. Curr. Opin. Chem. Eng. 2017;17(September):108–25. https://doi.org/10.1016/j.coche.2017.08.001.
[5] Gallucci F, Medrano JA, Fernandez E, Melendez J, Van Sint Annaland M, Pacheco-Tanaka DA. Advances on high temperature Pd-based membranes and membrane reactors for hydrogen purification and production. J. Membr. Sci. Res. 2017;3(3):142–56. https://doi.org/10.22079/jmsr.2017.23644.
[6] Gallucci F, Fernandez E, Corengia P, van Sint Annaland M. Recent advances on membranes and membrane reactors for hydrogen production. Chem Eng Sci 2013;92:40–66. https://doi.org/10.1016/j.ces.2013.01.008.
[7] Basile A, De Falco M, Iaquaniello G, Centi G. Part 1 fundamental studies on membrane reactor engineering. Membrane reactor engineering: applications for a greener process industry. John Wiley & Sons, Ltd.; 2016. p. 9.
[8] Basile A, De Falco M, Centi G, Iaquaniello G. Membrane reactor engineering. 2016.
[9] Alique D, Martinez-Diaz D, Sanz R, Calles JA. Review of supported pd-based membranes preparation by electroless plating for ultra-pure hydrogen production 2018;8(1).
[10] Cerrillo JL, et al. High purity, self-sustained, pressurized hydrogen production from ammonia in a catalytic membrane reactor. Chem Eng J 2022;431(December 2021). https://doi.org/10.1016/j.cej.2021.134310.
[11] Collins JP, et al. Catalytic dehydrogenation of propane in hydrogen permselective membrane reactors. Ind Eng Chem Res 1996;35(12):4398–405. https://doi.org/10.1021/ie960133m.
[12] Dittmeyer R, Höllein V, Daub K. Membrane reactors for hydrogenation and dehydrogenation processes based on supported palladium. J Mol Catal Chem 2001;173(1–2):135–84. https://doi.org/10.1016/S1381-1169(01)00149-2.
[13] Gallucci F, Basile A, Tosti S, Iulianelli A, Drioli E. Methanol and ethanol steam reforming in membrane reactors: an experimental study. Int J Hydrogen Energy 2007;32(9):1201–10. https://doi.org/10.1016/j.ijhydene.2006.11.019.
[14] Habib MA, et al. Palladium-alloy membrane reactors for fuel reforming and hydrogen production: a review. Energy Fuel 2021;35(7):5558–93. https://doi.org/10.1021/acs.energyfuels.0c04352.
[15] Iulianelli A, Ribeirinha P, Mendes A, Basile A. Methanol steam reforming for hydrogen generation via conventional and membrane reactors: a review. Renew Sustain Energy Rev 2014;29:355–68. https://doi.org/10.1016/j.rser.2013.08.032.
[16] Iulianelli A, Liguori S, Wilcox J, Basile A. Advances on methane steam reforming to produce hydrogen through membrane reactors technology: a review. Catal Rev - Sci Eng 2016;58(1):1–35. https://doi.org/10.1080/01614940.2015.1099882.
[17] Spallina V, et al. Direct route from ethanol to pure hydrogen through autothermal reforming in a membrane reactor: experimental demonstration, reactor modelling

and design. Energy 2018;143:666–81. https://doi.org/10.1016/j.energy.2017.11.031.
[18] Uemiya S, Sato N, Ando H, Matsuda T, Kikuchi E. Steam reforming of methane in a hydrogen-permeable membrane reactor. Appl Catal 1990;67(1):223–30. https://doi.org/10.1016/S0166-9834(00)84445-0.
[19] Bruni G, Rizzello C, Santucci A, Alique D, Incelli M, Tosti S. On the energy efficiency of hydrogen production processes via steam reforming using membrane reactors. Int J Hydrogen Energy 2019;44(2):988–99. https://doi.org/10.1016/j.ijhydene.2018.11.095.
[20] Ongis M, Di Marcoberardino G, Baiguini M, Gallucci F, Binotti M. Optimization of small-scale hydrogen production with membrane reactors. Membranes 2023;13(3):331. https://doi.org/10.3390/membranes13030331.
[21] Spallina V, Pandolfo D, Battistella A, Romano MC, Van Sint Annaland M, Gallucci F. Techno-economic assessment of membrane assisted fluidized bed reactors for pure H2 production with CO2 capture. Energy Convers Manag 2016;120:257–73. https://doi.org/10.1016/j.enconman.2016.04.073.
[22] Mosca L, et al. Process design for green hydrogen production. Int J Hydrogen Energy 2020;45(12):7266–77. https://doi.org/10.1016/j.ijhydene.2019.08.206.
[23] Lin YM, Liu SL, Chuang CH, Chu YT. Effect of incipient removal of hydrogen through palladium membrane on the conversion of methane steam reforming: experimental and modeling. Catal Today 2003;82(1–4):127–39. https://doi.org/10.1016/S0920-5861(03)00212-8.
[24] Yun S, Oyama ST. Correlations in palladium membranes for hydrogen separation: a review. J Membr Sci 2011;375:28–45. https://doi.org/10.1016/j.memsci.2011.03.057.
[25] Sholl DS, Lively RP. Seven chemical separations. Nature 2016;532:435–7.
[26] Bernardo P, Drioli E, Golemme G. Membrane gas separation: a review/state of the art. Ind Eng Chem Res 2009;48(10):4638–63. https://doi.org/10.1021/ie8019032.
[27] Al-Mufachi NA, Rees NV, Steinberger-Wilkens R. Hydrogen selective membranes: a review of palladium-based dense metal membranes. Renew Sustain Energy Rev 2015;47:540–51. https://doi.org/10.1016/j.rser.2015.03.026.
[28] Arratibel Plazaola A, Pacheco Tanaka DA, Van Sint Annaland M, Gallucci F. Recent advances in Pd-based membranes for membrane reactors. Molecules 2017;22(1):1–53. https://doi.org/10.3390/molecules22010051.
[29] Arratibel A, Pacheco Tanaka A, Laso I, van Sint Annaland M, Gallucci F. Development of Pd-based double-skinned membranes for hydrogen production in fluidized bed membrane reactors. J Membr Sci 2018;550(August 2017):536–44. https://doi.org/10.1016/j.memsci.2017.10.064.
[30] Arratibel A, Medrano JA, Melendez J, Pacheco Tanaka DA, van Sint Annaland M, Gallucci F. Attrition-resistant membranes for fluidized-bed membrane reactors: double-skin membranes. J Membr Sci 2018;563(June):419–26. https://doi.org/10.1016/j.memsci.2018.06.012.
[31] H2SITE inaugurates the first production plant for palladium alloy membranes to obtain hydrogen. Businesswire; 2022 [Online]. Available: https://www.businesswire.com/news/home/20221115005287/en/H2SITE-inaugurates-the-first-production-plant-for-palladium-alloy-membranes-to-obtain-hydrogen [Accessed: 27-Mar-2023].
[32] Gallucci F. In: Drioli E, Giorno L, editors. Richardson law. Encyclopedia of membranes. Berlin, Heidelberg: Springer Berlin Heidelberg; 2012. p. 1–2.

[33] Melendez J, Fernandez E, Gallucci F, van Sint Annaland M, Arias PL, Pacheco Tanaka DA. Preparation and characterization of ceramic supported ultra-thin (~1 μm) Pd-Ag membranes. J Membr Sci 2017;528(October 2016):12–23. https://doi.org/10.1016/j.memsci.2017.01.011.

[34] Flanagan TB, Wang D. Exponents for the pressure dependence of hydrogen permeation through Pd and Pd-Ag alloy membranes. J Phys Chem C 2010;114(34):14482–8. https://doi.org/10.1021/jp101364j.

[35] Caravella A, Hara S, Drioli E, Barbieri G. Sieverts law pressure exponent for hydrogen permeation through Pd-based membranes: coupled influence of non-ideal diffusion and multicomponent external mass transfer. Int J Hydrogen Energy 2013;38(36):16229–44. https://doi.org/10.1016/j.ijhydene.2013.09.102.

[36] Brencio C, Fontein FWA, Medrano JA, Di Felice L, Arratibel A, Gallucci F. Pd-based membranes performance under hydrocarbon exposure for propane dehydrogenation processes: experimental and modeling. Int J Hydrogen Energy 2022;47(21):11369–84. https://doi.org/10.1016/j.ijhydene.2021.09.252.

[37] Arratibel A, Astobieta U, Pacheco Tanaka DA, Van Sint Annaland M, Gallucci F. N2, He and CO2 diffusion mechanism through nanoporous YSZ/γ-Al2O3 layers and their use in a pore-filled membrane for hydrogen membrane reactors. Int J Hydrogen Energy 2016;41(20):8732–44. https://doi.org/10.1016/j.ijhydene.2015.11.152.

[38] Nordio M, et al. Effect of sweep gas on hydrogen permeation of supported Pd membranes: experimental and modeling. Int J Hydrogen Energy 2019;44(8):4228–39. https://doi.org/10.1016/j.ijhydene.2018.12.137.

[39] Boon J, Li H, Dijkstra JW, Pieterse JAZ. 2-Dimensional membrane separator modelling: mass transfer by convection and diffusion. Energy Proc 2011;4:699–706. https://doi.org/10.1016/j.egypro.2011.01.108.

[40] Ververs WJR, Arratibel A, Di Felice L, Gallucci F. Dataset - results permeation tests double-skin Pd-based membranes, conventional Pd-based membranes and porous membranes. Zenodo; 2024. https://doi.org/10.5281/zenodo.10691625.

[41] Arratibel A, Pacheco Tanaka A, van Sint Annaland M, Gallucci F. On the use of double-skinned membranes to prevent chemical interaction between membranes and catalysts. Int J Hydrogen Energy 2021;46(38):20240–4. https://doi.org/10.1016/j.ijhydene.2019.10.203.

[42] Ho CK, Webb SW. Gas tranport in porous media. Springer; 2006.

[43] Veldsink JW, van Damme RMJ, Versteeg GF, van Swaaij WPM. The use of the dusty-gas model for the description of mass transport with chemical reaction in porous media. Chem Eng J Biochem Eng J 1995;57(2):115–25. https://doi.org/10.1016/0923-0467(94)02929-6.

[44] Boon J, Pieterse JAZ, Dijkstra JW, van Sint Annaland M. Modelling and systematic experimental investigation of mass transfer in supported palladium-based membrane separators. Int J Greenh Gas Control 2012;11(SUPPL):122–9. https://doi.org/10.1016/j.ijggc.2012.09.014.

[45] Mason EA, Malinauskas AP. Gas tranport in porous media: the dusty-gas model. Chemical engineering monographs. 1983.

[46] Do DD. Fundamentals of diffusion and adsorption, vol. 2. Porous Media; 1998.

[47] Ververs WJR, Ongis M, Arratibel A, Di Felice L, Gallucci F. On the modeling of external mass transfer phenomena in Pd-based membrane separations. Int J Hydrogen Energy 2024.

[48] Poling BE, Prausnitz JM, O'Connell JP. Properties of gases and liquids. 2013.

[49] Reid RC, Praunitz JM, Poling BE. The properties of gases and liquids. fourth ed. New York: McGraw-Hill; 1987.

[50] Bird RB, Stewart WE, Lightfoot EE. Transport phenomena. second ed. John Wiley & Sons, Inc.; 2002.